Exploring the Mechanical Stability of the C2 Domains in Human Synaptotagmin 1

Li Duan,[†] Artem Zhmurov,[‡,§] Valeri Barsegov,[‡,§] and Ruxandra I. Dima[*,†]
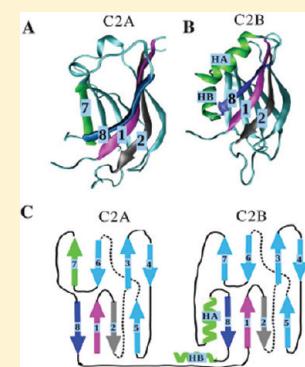
[†]Department of Chemistry, University of Cincinnati, Cincinnati, Ohio 45221, United States
[‡]Department of Chemistry, University of Massachusetts, Lowell, Massachusetts 01854, United States
[§]Moscow Institute of Physics and Technology, Moscow Region, Russia 141700

S *Supporting Information*

ABSTRACT: Human synaptotagmin 1 (Syt1) plays a crucial role in the bending of the membrane during neurotransmitter release at the synapse. Hence, resolving the structural details of Syt1 that underlie its biological function is fundamental for providing mechanistic insights into the nature of the synaptic response. We explored the unfolding micromechanics of Syt1 by analyzing the free energy landscape of the whole molecule and its C2A and C2B domains. We employed a self-organized polymer (SOP) model of a protein chain to carry out pulling simulations, accelerated on graphics processing units (GPUs), under experimental force loads. To resolve the atomic-level details, we complemented the SOP model simulations with atomistic simulations. On the basis of the results obtained, we hypothesize that (1) isolated single domains C2A and C2B present similar mechanical resistance against an applied pulling force but unfold following different kinetic pathways and that (2) C2B is more mechanically resistant in the C2AB complex due to stabilizing interactions with other domains. These findings correlate well with recent atomic force microscopy (AFM) studies on the Syt1 molecule, in which the increase in the unfolding force for C2B was detected when this domain was joined with C2A. Our results also suggest that the linkers (I27 domains) used in the experimental setup can modulate the mechanical behavior of this synaptic protein complex and alter not only the critical force for unfolding but also the unfolding pathways for the C2 domains. Interestingly, the presence of the C2A–C2B domain interface in the C2AB complex confers mechanical stability to either of the C2 domains. Our findings provide new insights into the relative conformational variability of the C2 domains, which we believe to be modulated, to a large extent, by intermolecular coupling with other proteins.

■ INTRODUCTION

Membrane fusion occurs through formation of a close contact between two lipid bilayers, followed by the local distortion of each bilayer, and formation of a single, merged membrane. Proteins play key roles in these processes, especially in generating and controlling the elastic stress exerted on the membrane. The critical step in the initiation of lipid rearrangements by the fusion proteins is local bending of membrane bilayers into dimples pointing toward the adjacent membrane.[1] Membrane bending results in bringing the membrane bilayers into close contact and in priming the protein-depleted, stressed tops of the bilayer bulges by lowering the energy barriers for hemifusion and pore opening. In neuronal membrane fusion, neurotransmitter release at the synapse is mediated by the Ca^{2+}-induced fusion of transmitter-loaded synaptic vesicles with the presynaptic plasma membrane. Experiments show that the Ca^{2+} sensor, required for fast fusion, is synaptotagmin-1 (Syt1), which binds to the SNARE complex and induces the buckling of the plasma membrane.[2] Syt1 has a short N-terminal luminal domain, a transmembrane domain, and a C-terminal cytoplasmic region composed of two domains, C2A and C2B, forming the C2AB complex. These domains bind Ca^{2+} ions and induce monolayer bending due to the mechanical tension created by the insertion of

their Ca^{2+} binding loops into the lipid monolayer. McMahon and collaborators[2] measured the extent of buckling of the membrane induced by Syt1, and observed a $\sim 20k_BT$ decrease in the activation barrier for the membrane-membrane fusion. Cafiso and co-workers[3] found that the C2AB complex inserts about 10 Å into the membrane, which results in forces of ~ 80 pN. Recently, Takahashi et al.[4] measured the force required to extract the C2AB complex from lipid bilayers, using single-molecule AFM experiments. The forces of ~ 73 pN and 122 pN reported by Takahashi et al.[4] agree with the force estimates based on the results of Cafiso et al.[3] These recent findings show that the Syt1-induced membrane bending is a mechanically regulated process, in which large force loads are exerted on the Syt1 molecule. Hence, resolving the mechanical properties of Syt1, especially of its C-terminal region (C2AB complex), is crucial for understanding its role in synaptic fusion.

Single-molecule atomic force microscopy (AFM) measurements have been used to explore the physical properties of human Syt1. By applying the constant velocity pulling technique

(force-ramp) to linear tandems of C2A domains of Syt1, Carrion-Vazquez et al.[5] found that these domains unfold independently and resist to pulling forces of ∼60 pN. In a recent AFM study on the C2AB complex (279 amino acid residues),[6] sandwiched between $(I27)_2$ constructs, Fuson et al.[7] found that, despite large structural similarity shared by their native folds, the domains C2A and C2B are characterized by markedly different mechanical properties. The C2A domain unfolds at an average force of ∼50 pN, whereas the C2B domain yields to higher average force of ∼100 pN.[7] These values agree with the range of forces found by Takahashi et al.,[4] and also correlate with the biochemical data of Gaffney et al. in that the single C2A domain does not retain the functional activity of the C2AB complex.[8] However, the AFM assays performed by Takahashi et al.[4] and Fuson et al.[7] differ in that the former study referred to the C2AB complex attached to lipid bilayers, whereas the latter addressed the mechanical behavior of the C2A domain and the C2AB complex. In addition, the AFM measurements of Takahashi and co-workers[4] revealed that domains C2A and C2B require comparable forces of 54−102 pN and 73 pN, respectively, to break from the bilayer. In their AFM experiments, Fuson et al.[7] also performed force measurements on the isolated single C2A domain, sandwiched between the tandems of I27 domains and found that C2A unfolds according to two distinct pathways. Importantly, ∼40% of the time C2A unfolded by populating an intermediate partially unfolded state. The formation of this intermediate conformation was hypothesized to result from the mechanical unraveling of the first two β-strands, S1 and S2.[7] Moreover, Fuson et al.[7] attributed the increased mechanical stability of the C2B over the C2A domain to the presence of the additional HA helix near the C-term end of C2B.

Although AFM-based dynamic force measurements have provided valuable insight into the mechanical response of the C2AB complex to an applied pulling force, these experiments alone cannot reveal the microscopic structural basis underlying the physical properties of the biologically important fragment of Syt1. Molecular simulations play an important role in providing unique information about structural changes that accompany unfolding transitions in proteins at the microscopic level. Steered molecular dynamics (SMD) simulations are crucial in resolving the atomic-level underpinnings underlying forced unraveling of the secondary structure elements.[9] For example, SMD simulations of the C2A domain in explicit solvent have shown that forced unfolding of the C2A domain occurs through initial unzipping of the hydrogen bonds connecting the S1 and S8 strands at the N- and C-terminal ends.[7,10] However, the mechanical properties of soft biological matter critically depend on precise conditions of the time-dependent force application, $f(t) = r_f t$, including the force-loading rate $r_f = k_s v_f$ or pulling speed v_f (k_s is the cantilever spring constant).[11] Although all-atomic models do reproduce some of the features of mechanical unfolding of Syt1, it is virtually impossible to characterize the complex kinetics and unfolding mechanism(s) for Syt1, subject to the experimentally relevant force-loads, using all-atomic modeling alone. Here, we employed a combination of all-atom MD simulations in implicit water and a simplified description of proteins (coarse-grained model) to explore the unfolding nano-mechanics for the C2AB complex.

We used the EEF1 model of implicit solvation[12] to parametrize the self-organized polymer (SOP) model[13] of the C2AB complex, which was then used to carry out pulling simulations accelerated on graphics processing units (GPUs). The EEF1 model retains the atomistic description of a protein chain but describes solvent as a Gaussian-distributed average contribution.[12] This model has been successfully employed in the past by other groups to probe the mechanical response for a number of proteins.[14−16] To evaluate the robustness of the mechanical unfolding results to changes in the treatment of the solvent contribution, we also carried out a set of simulations using a different implicit solvent model, the generalized Born (GBSW) model.[17] Employing the SOP model enabled us to perform dynamic force measurements in silico on the experimental centisecond time scale using experimental pulling speeds (v_f = 1−25 μm/s). The coarse-grained SOP model has proved to be successful at describing the physical properties of proteins, including the tubulin dimer,[18] kinesin,[19] and green fluorescent protein.[20] This model has been used to explore the kinetics and to map the free energy landscape of myosin V,[21] protein kinase A,[22] riboswitch aptamers,[23] DHFR,[24] and GroEL.[25] Similar minimalist approaches have been employed by researchers to probe the mechanical properties of the C2A domain and other proteins.[26,27] To speed up computations, we utilized molecular simulations fully implemented on graphics processors.[11] GPUs are being utilized in compute-intensive, highly parallel scientific calculations performed on many computational cores or Arithmetic Logic Units (ALUs). Because GPU-based simulations are oftentimes 10−250 times faster than some of the optimized CPU-based methods, GPUs are being used as performance accelerators in a range of scientific applications including the biological N-body problem.[28−30] In this study, GPUs have been used to carry out long pulling simulations of the C2AB complex and the tandem of C2A domains, C2A−C2A. These efforts allowed us to gather a representative set of unfolding data for each system and to arrive at statistically significant conclusions.

Due to the vectorial nature of the mechanical perturbation, an application of a pulling force results in the projection of the multidimensional energy landscape on a particular reaction coordinate for unfolding.[31] To compare directly the simulation results with the experimental force spectra, in dynamic force measurements in silico, we implemented the pulling setup used in AFM experiments,[5,7] in which the mechanical force-ramp $f(t)$ was applied along the end-to-end vector of the polypeptide chain connecting the N- and C-termini. In addition, following the experimental conditions, we did not include Ca^{2+} ions in our simulations. Here, we briefly summarize the main results. Our simulation results suggest that isolated single domains C2A and C2B have comparable mechanical resistances and unravel predominantly from their C-terminal (C-term) ends, following different pathways due to kinetic partitioning. Because the mechanical behavior of the isolated C2B domain has not yet been characterized, our theoretical findings may serve as a starting point for future experimental studies. Our own results lead us to propose an alternative explanation for the enhanced mechanical stability of the C2B domain compared to the C2A domain, observed experimentally for the C2AB complex.[7] Specifically, rather than resulting from stabilizing interactions between the HA helix and the rest of the molecule, the mechanical stability of C2B may come from favorable interactions between the C2B domain and the covalently linked I27 domain, which binds to the "bottom face" of C2B opposed to the Ca^{2+}-binding loops.[32] Finally, we found that, combining the two C2 domains (C2A and C2B) in the C2AB complex with a stable interface at the C2A−C2B junction results in higher critical forces for unfolding for both domain and the emergence of a new unfolding

pathway, in which C2A unravels from the N-term end. This kinetic switch in unfolding pathways is quite similar to the kinetic partitioning observed in the tubulin dimer[18,33] and is a direct outcome of the dynamic competition between tension propagation in the protein chain and binding interactions among the residues that stabilize the interface between the domains C2A and C2B, or between the C2 domains and other proteins. Interestingly, the pathway switch is controlled by the C-term β-strand of the C2A domain, which might become destabilized by thermal agitations in the protein chain. Because all our predictions are amenable to experimental testing, we anticipate that these predictions will stir single-molecule studies to fully characterize the mechanical behavior of the Syt1 molecule.

■ METHODS

Self-Organized Polymer (SOP) Model. We used the SOP model, which is based on the native topology of a protein. In this model, each amino acid residue in the crystal structure of Syt1 (PDB entry 2R83) is represented by its C_α atom.[13] The total potential energy function for a protein conformation, specified in terms of the coordinates $\{r_i\}$ ($i = 1, 2, ..., N$), where N is the total number of residues, is given by

$$V_T = V_{FENE} + V_{NB}^{ATT} + V_{NB}^{REP}$$

$$= -\sum_{i=1}^{N-1} \frac{k}{2} R_0^2 \log\left(1 - \frac{(r_{i,i+1} - r_{i,i+1}^o)^2}{R_0^2}\right)$$

$$+ \sum_{i=1}^{N-3} \sum_{j=i+3}^{N} \varepsilon_h \left[\left(\frac{r_{ij}^o}{r_{ij}}\right)^{12} - 2\left(\frac{r_{ij}^o}{r_{ij}}\right)^6\right] \Delta_{ij}$$

$$+ \sum_{i=1}^{N-2} \varepsilon_l \left(\frac{\sigma_{i,i+2}}{r_{i,i+2}}\right)^6 + \sum_{i=1}^{N-3} \sum_{j=i+3}^{N} \varepsilon_l \left(\frac{\sigma}{r_{ij}}\right)^6 (1 - \Delta_{ij})$$

(1)

In eq 1, the distance between any two interacting residues i and $i + 1$ is $r_{i,i+1}$, and $r_{i,i+1}^o$ is the corresponding value in the native structure. The first term in eq 1 is the backbone chain connectivity potential. The second term accounts for the noncovalent interactions that stabilize the native (folded) state. If the noncovalently linked residues i and j ($|i - j| > 2$) are within a cutoff distance R_C (i.e., $r_{ij} < R_C = 8$ Å), then $\Delta_{ij} = 1$, and zero otherwise. A uniform value of $\varepsilon_h = 0.9$ kcal/mol, which quantifies the strength of nonbonded interactions, was assumed for each domain (C2A and C2B). We selected this value on the basis of the results of the atomistic MD simulations. The native state energy for C2A and C2B is −348 and −498 kcal/mol, and the number of native contacts is 400 and 514, respectively. Hence, the average energy per contact is ∼0.9 kcal/mol. For the I27 domains we used $\varepsilon_h = 1.25$ kcal/mol.[11] All the non-native interactions, described by the third and fourth terms in eq 1, are treated as repulsive. Also, in eq 1, $R_0 = 2$ Å and $\varepsilon_l = 1$ kcal/mol. For the binary contacts at the interface between any two domains D1 and D2 forming the C2AB complex (C2A and C2B) or in tandem $(I27)_2−C2AB−(I27)_2$ (C2A, C2B, and I27), we used the Lorentz−Berthelot mixing rule, $\varepsilon_h^{int} = (\varepsilon_h^{D1} \varepsilon_h^{D2})^{1/2}$.

Simulation Details. We carried out Langevin simulations for all the systems at room temperature ($T = 300$ K). The integration time step h was computed as $h = 0.16\tau_H$, where $\tau_H = \zeta \varepsilon_h \tau_L / k_B T$ is the characteristic time for Brownian motion.[34] Here, $\zeta = 50$, the

unitless friction coefficient, accounts for the high friction regime (overdamped limit), τ_L is the time scale for Langevin dynamics, and $k_B T$ is the thermal energy ($k_B T = 0.6$ kcal/mol at $T = 300$ K). Depending on the protein in question, in the high friction regime τ_L varies between 2 and 3 ps.[13,18,24] This leads to the integration time step of 27−40 ps. To mimic the experimental force-ramp measurements, we applied the time-dependent pulling force $f(t) = k_s v_f t$ to the C-term end of each system (tagged residue) moving it with the constant speed (v_f) in the direction of the end-to-end vector, while keeping the N-term end fixed (constrained residue). The cantilever spring constant was set to $k_s = 35$ pN/nm, which is within the experimental ∼10−100 pN/nm range used in AFM. The details of the pulling simulations are given in section 1 of the Supporting Information. Summarized description of the simulation procedures, including types of molecules, structural models, computational methods, constrained and tagged residues, pulling speeds, time scales, number of simulation runs, are summarized in Table 1 in the Supporting Information. The intermediate states were identified by comparing the global rmsd values ($\Delta_{WT}(t)$) and the partial rmsd values ($\Delta_\Omega(t)$).[18] These measures of structural similarity between the wild-type (WT) or native structure and transient structures (Ω) were used to estimate the time at which a secondary structure element detached from the rest of the molecule.[20] Transient conformations were identified by evaluating the percentage of exposed hydrophobic residues. In dynamic force measurements in vitro, the unfolding peaks can be detected only when this ratio does not exceed 45%. We used MaxSprout[35] to reconstruct the molecules in atomistic detail starting from their reduced C_α-atom based structures. The description of procedure used in MD simulations in implicit solvent is presented in section 2 in the Supporting Information (see, also, Table 1 in Supporting Information section 1).

Full Go Approach. In the original SOP model,[13] which we refer to as the Simple-Go (SG) model, the native contacts are pairs of residues whose C_α-atoms are within the cutoff distance $R_C = 8$ Å (Lennard-Jones potential in eq 1). To characterize the C2A−C2B and C2B−I27 domain interactions in the C2AB complex and in the tandem $(I27)_2−C2AB−(I27)_2$, we extended the SG model to include the noncovalent intermolecular coupling. This can be achieved by taking into account all the pairwise interactions between amino acids, for which their heavy atoms are within a given cutoff distance. In this approach, the contacts consist of residue pairs for which either their C_α-atoms are within 8 Å distance or heavy atoms in their side chains are within 5.2 Å distance.[36] We refer to this approach as the Full Go (FG) model. Considering the interface between the C2A and C2B domains (C2AB complex), the salt bridges between residues Asp178 (in C2A) and Arg388 (in C2B) and between residues Arg199 and Arg233 (in C2A) and Asp392 (in C2B) stabilize the C2A−C2B interface.[6] The side chains associated with these pairs of positions are in contact (within 3 Å), while the distance between their C_α-atoms exceeds R_C. Hence, while in the SG model these binding interactions are treated as neutral, in the FG approach these contacts stabilizing the C2A−C2B interface are accounted for. In all the SOP-model based simulations, we utilized the FG description of nonbonded interactions (see, also, Table 1 in Supporting Information).

CPU-Based and GPU-Based Simulations. We employed a combination of pulling simulations on a CPU and on a GPU to generate statistically representative sets of unfolding trajectories for the whole C2AB molecule, the $(I27)_2−C2AB−(I27)_2$

10135

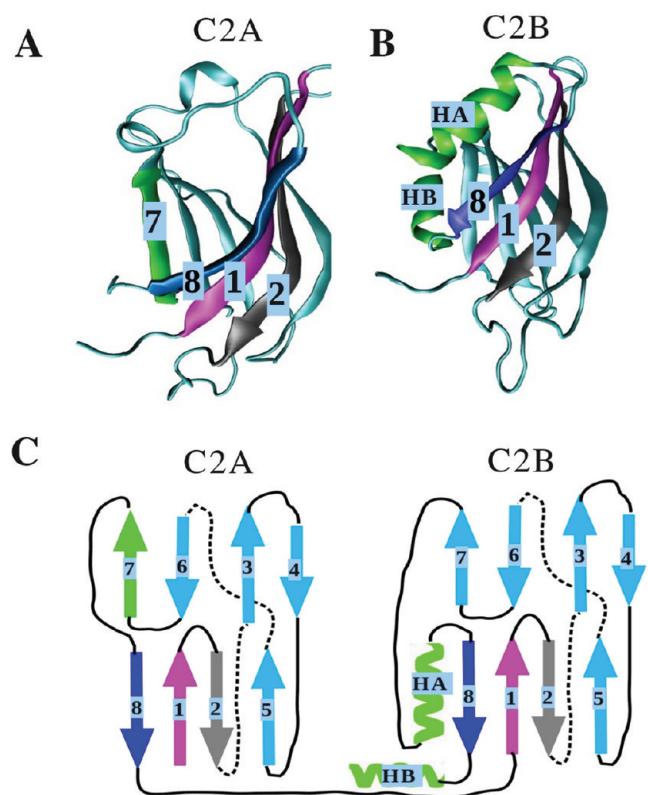dx.doi.org/10.1021/jp2025945 |J. Phys. Chem. B 2011, 115, 10133–10146

Figure 1. Structural representation of the C2A domain (panel A), C2B domain (panel B), and the native topology of the C2AB complex (panel C) obtained from the PDB file 2R83 using VMD[46] and PovRay packages. The β-strands S1—S8 in the C2A domain, and the β-strands S1—S8 and helices HA and HB in the C2B domain are indicated.

construct, and for separated single domains C2A and C2B. Given their large size (130—630 residues), we utilized GPU-based computations to carry out long pulling simulations for larger systems: the C2AB complex, the $(I27)_2$—C2AB—$(I27)_2$ construct, and the C2A dimer (C2A—C2A). We utilized graphics cards GeForce GTX 280 and GTX 295 (from NVIDIA), which have one and two GPUs per card with a total of 240 ALUs (30 multiprocessors) and 480 ALUs (60 multiprocessors), respectively. To perform pulling simulations on the experimental time scale, we have developed and tested a GPU-based implementation of Langevin dynamics simulations by adapting the SOP model (SOP-GPU package).[11] All the steps of the algorithm, including generation of (pseudo)random numbers (for calculation of random forces), evaluation of the potential energy terms (eq 1) and molecular forces, generation of Verlet lists, and numerical integration of Langevin equations of motion, have been converted into a standard CUDA code (section 3 in Supporting Information).

■ RESULTS

In the PDB file 2R83, the C2A domain (residues 140—265) is composed of eight β-strands S1—S8 and the α-helix H1 (Figure 1A). The C2B domain (residues 271—418) consists of eight β-strands S1—S8 and two helices HA and HB (Figure 1B). The linker between the C2A and C2B domains spans positions 266—270. Using the SOP model, we carried out pulling simulations for the isolated single domains C2A and C2B, for the C2A dimer, and for the C2AB complex using the experimental pulling

speed v_f = 2.5 μm/s (loading rate r_f = 8.75 $\times$ 10^4 pN/s) and v_f = 25 μm/s (r_f = 8.75 $\times$ 10^5 pN/s). To characterize atomic-level contributions to the unfolding pathways, we carried out GBSW-model based simulations for the isolated C2B domain, and EEF1-model based simulations of the isolated domains C2A and C2B and for the C2AB complex (Table 1 in Supporting Information).

C2A Unfolds through Competing Pathways. In very good agreement with the experimental results,[7] our simulations reveal that the isolated C2A domain unfolds following two distinct pathways. Out of 95 trajectories obtained at v_f = 2.5 μm/s, 32 trajectories (34%) followed the minor pathway 1 (Figure 2A), whereas 63 trajectories (66%) followed the major pathway 2 (Figure 2B). These results agree with the experimental results,[7] according to which in the minor pathway 1, observed ~38% of the time, C2A unravels by populating an intermediate state. We next analyzed the unfolding force signals (peak maxima) observed in the simulated force—extension curves (FECs). For the minor pathway 1 (Figure 2A), we observed a single force signal (peak 1), which corresponds to the formation of the intermediate state. This transition (Figure 2C, structure 1) is due to the unraveling of the C-term strand S8 at an average peak force of 56.2 $\pm$ 4.1 pN (C2A simulations; Table 1). In agreement with the results of SMD simulations,[5] unfolding of S8 is accompanied by the force-induced rupture of the contacts connecting S8 with S1 and by the alignment of the remaining part of the molecule along the direction of pulling force. Figure SI1A in Supporting Information further shows a sequence of unfolding events observed for pathway 1 for the trajectory displayed in Figure 2A in terms of unfolding forces and partial rmsd values (see Methods). At $t \approx$ 5.2 ms, the strands S1 and S7 detach from the rest of the C2A molecule (Figure 2C, structure 2), at an average peak force of 60.3 $\pm$ 6.0 pN (Table 1). This is the last experimentally detectable force peak 2 for pathway 1. Here, the remaining part of C2A is severely distorted, resulting in the rmsd exceeding 5.0 nm, and the ratio of hydrophobic residues exposed to solvent exceeds 41.5%. Hence, additional intermediate conformations observed in pulling simulations are short-lived and, thus, are not detected experimentally.[20] The ~6.9 nm peak-to-peak distance between the peaks 1 and 2 (Figure 2A) is within the 7.4 $\pm$ 3.5 nm extension measured experimentally (see Figure 3C in ref 7). For the major pathway 2 (Figure 2B), the forced unfolding is initiated by unraveling of the S8 strand at $t \approx$ 2.0 ms (Figure 2D, structure 1) at an average force of 57.4 $\pm$ 3.5 pN (Table 1). The second peak at a force of ~50 pN is due to the detachment of the strand S7, followed by the unraveling of the strand S6 (Figure 2D, structure 2). However, this peak is not detectable because, upon stretching of S8, the ratio of exposed hydrophobic residues reaches ~56%. This suggests that although in both pathways the same strand (S8) detaches, the remainder of C2A is more distorted in pathway 2. For both pathways, the full extension of the C2A domain is ~40 nm.

The histogram of unfolding forces for each pathway (Figure 2E,F) shows a 45—75 pN force range (peaks 1 and 2), which is within the experimentally determined distribution of forces for the C2A monomer (see Figure 3C in ref 7). The stochastic variability in unfolding forces is illustrated in Figure 2G,H, where we superposed the force—extension traces from several trajectories. To better compare the experimental and simulation data, we also conducted 50 pulling simulations for the single C2A domain at a higher pulling speed v_f = 25 μm/s.
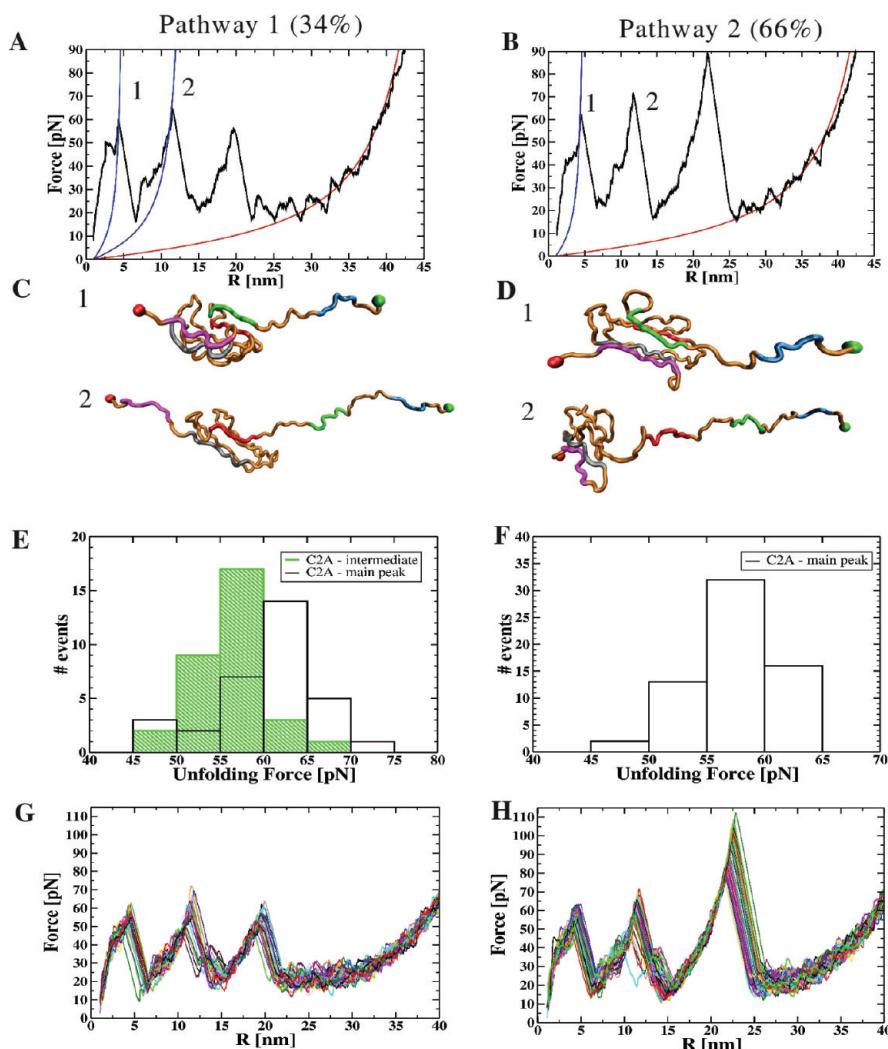
Figure 2. Force-induced unfolding of the isolated single C2A domain. The theoretical force−extension curves (FECs, black rugged lines) for the unfolding pathway 1 (panel A) and pathway 2 (panel B) show the consecutive unfolding transitions. In this figure, and in Figures 2−8, thick ascending curves represent worm-like chain (WLC) fits to the simulated force spectra (blue lines). The structural snapshots for pathway 1 and 2 in panels C and D correspond to the force peaks labeled 1 and 2 in panels A and B, respectively. Peak 2 (panel A) corresponds to the intermediate state (structure 2) detected in pathway 1. Additional peaks observed in the theoretical FECs are not detectable experimentally (see main text for details). The theoretical FECs should be compared with the experimental force spectra (Figure 3 in ref 7). The rightmost WLC curves (red line) correspond to stretching of the fully unfolded C2A domain. In pathway 1, the C2A domain unfolds at an average force of 56.2 ± 4.1 pN (intermediate peak) and 60.3 ± 6.0 pN (last detectable peak). In pathway 2, the C2A domain unfolds at an average force of 57.4 ± 3.5 pN, which is the only detectable peak. The histograms of peak forces, showing the main and intermediate transitions for pathways 1 and 2, are presented in panels E and F, respectively. In panels G and H, the simulated force spectra obtained from several trajectories for pathway 1 and 2 are overlaid for comparison.

At a faster force load, we observed the same two pathways 1 (36%) and pathway 2 (64%), characterized by slightly higher values of unfolding forces, which was expected. For example, the average first (second) force peak has increased to 69.3 ± 7.5 pN (73.3 ± 9 pN), in full agreement with experiments (see Figure 4C in ref 7). We also carried out pulling simulations for the dimer C2A−C2A (C2A−C2A simulations; Table 1) formed by linked C2A domains (see, also, section 4 in Supporting Information), and obtained a good agreement (Figures SI2 and SI3 in Supporting Information) with experimental data.[5] More-over, in this set of simulations we observed a new pathway 3 for unfolding of the C2A domain in addition to pathways 1 and 2 (S2A simulations), which corresponds to a single-step unrav-eling of C2A from the N-term end (Figure SI3, Supporting Information).

Unfolding of C2B Is an All-or-None Process. Based on the structural similarity shared by the C2B and C2A domains, it is reasonable to expect similar bifurcation in the unfolding path-ways for the C2B domain. However, we found that unfolding of C2B is an all-or-none process, with no kinetic partitioning (Figure 3A). In all 48 simulation runs (C2B simulations; Table 1), the C2B domain unfolded from the C-term end (unraveling of the HB helix), with no experimentally detectable force signal, which results in a molecular extension of ∼3.4 nm. This is followed by the partial unraveling of the strand S1 at the N-term end, which peels off from the strands S2 and S8 (Figure 3C, structure 1). Then, the unfolding transitions that follow, i.e., simultaneous unraveling of the S8 strand and HA helix (Figure 3C, structure 2), occur at the opposite (C-term) end of the chain, giving rise to the first force signal of 68 pN at an

Table 1. Average Forces, Average Extensions, and Unfolding Pathways Obtained from Pulling Simulations for the Syt1-Derived Molecular Fragments (See, Also, Table 1 in the Supporting Information)[a]

simulations[b]	unfolding pathway[c]-domain (motif)[d]	force, pN	extension, nm
C2A	P1—S8	56.2 ± 4.1	7.0 ± 0.3
	P1-whole domain	60.3 ± 0.6	39.7 ± 0.4
	P2	57.4 ± 3.5	39.5 ± 0.3
C2A—C2A	P3	63.3 ± 3.9	39.5 ± 0.2
C2B	HB	-	3.4 ± 0.5
	whole domain	63.8 ± 4.2	44.5 ± 0.5
C2A(EEF1)	P1—S8	240.3 ± 33.1	7.8 ± 1.4
	P1 or P2-whole domain	261.3 ± 53.3	40.1 ± 2.0
	P3	232.3 ± 39.2	39.7 ± 1.5
C2B(EEF1)	P1	241.0 ± 32.1	44.5 ± 2.1
	P2	271.4 ± 39.2	44.3 ± 1.9
C2B(GBSW)	P1	319.7	44.5
	P2	370.2	44.3
C2AB(EEF1)	C2A	341.3 ± 35.2	40.3 ± 0.5
	C2B	367.3 ± 64.8	45.0 ± 0.4
C2AB	P1—C2A	97.1 ± 6.4	37.2 ± 1.2
	P1—C2B	54.0 ± 0.1	44.9 ± 1.2
	P2—C2A	97.7 ± 6.9	38.0 ± 1.0
	P2—C2B	57.8 ± 3.4	44.7 ± 0.9
	P3—C2B	96.3 ± 6.4	43.3 ± 1.1
	P3—C2A-S8	67.1 ± 3.3	7.2 ± 1.6
	P3—C2A-whole domain	62.3 ± 5.2	38.1 ± 1.1
C2A—C2B	C2A-S8	63.2 ± 4.5	7.4 ± 0.3
	C2A-whole domain	61.9 ± 5.2	38.3 ± 0.9
	C2B	59.7 ± 3.7	44.6 ± 1.0
C2AB—I27	P1—C2A	92.7 ± 8.6	37.9 ± 0.5
	P1—C2B	116.0 ± 7.6	44.5 ± 0.9
	P2—C2A	98.8 ± 5.8	37.5 ± 1.0
	P2—C2B	113.3 ± 9.6	45.0 ± 1.1
	P3—C2B	96.7 ± 6.5	44.7 ± 1.2
	P3—C2A	72.9 ± 7.0	37.6 ± 0.8
C2A—C2B—I27	C2A-S8	55.1 ± 5.7	7.5 ± 1.2
	C2A-whole	58.4 ± 8.0	38.0 ± 1.5
	C2B	116.7 ± 8.5	45.2 ± 1.5
	I27	220.4 ± 10.3	28.6 ± 1.7

[a] Notations for domains and secondary structure elements are the same as in Figure 1. [b] Different simulation types described in the Results. The entries containing EEF1 (GBSW) refer to the results obtained from the EEF1 (GBSW)-model based simulations; the other entries refer to pulling simulations performed using the SOP-model. C2AB and C2A—C2B refer, respectively, to pulling simulations for the C2AB complex with the C2A—C2B association interface ("closed" conformation) and for the C2AB complex with no C2A—C2B domain interactions ("open" conformation). [c] P1 = pathway 1, P2 = pathway 2, and P3 = pathway 3. [d] Domain or secondary structure element that unravels along this pathway.

average ∼5.2 nm extension (Table 1). Next, either S7 and S1 unfold (∼75% of trajectories) or S7 and S6 unfold (∼25% of trajectories), but these transitions are not detectable experimentally because the ratio of exposed hydrophobic residues reaches 63.5% upon unraveling of HB, S8, and HA (first peak). Hence, we conclude that, in our simulations, the forced unfolding of the C2B domain is an "all-or-none" transition, which occurs at an average force of 63.8 ± 4.2 pN (Figure 3B) and results in an overall extension of 44.5 nm (Table 1). Importantly, this type of "all-or-none" transition observed in C2B is also consistent with the results of Fuson et. al[7] for the C2AB complex. In agreement with Fuson et al.,[7] we found that the contribution of the HB helix to the mechanical stability of C2B is, indeed, negligible. To further validate this result, we performed pulling simulations for

the C2B domain without the HB helix at the C-term end of C2B. We found that this deletion does not alter the all-or-none character of unfolding of C2B and does not change the magnitude (height) nor location (extension) of the force signal (data not shown).

C2A—C2B Interface Enhances the Mechanical Resistance of C2 Domains. Experimental AFM studies have demonstrated that domain interactions between adjacent protein repeats in multimeric proteins (tandems) modulate their mechanical properties.[37] For the C2AB complex, Fuson et al.[7] have reported considerably higher unfolding forces for the C2B domain compared to the C2A domain. These forces (∼100 pN) are also larger than the unfolding forces obtained from our pulling simulations for the isolated C2B domain (64 pN; C2B
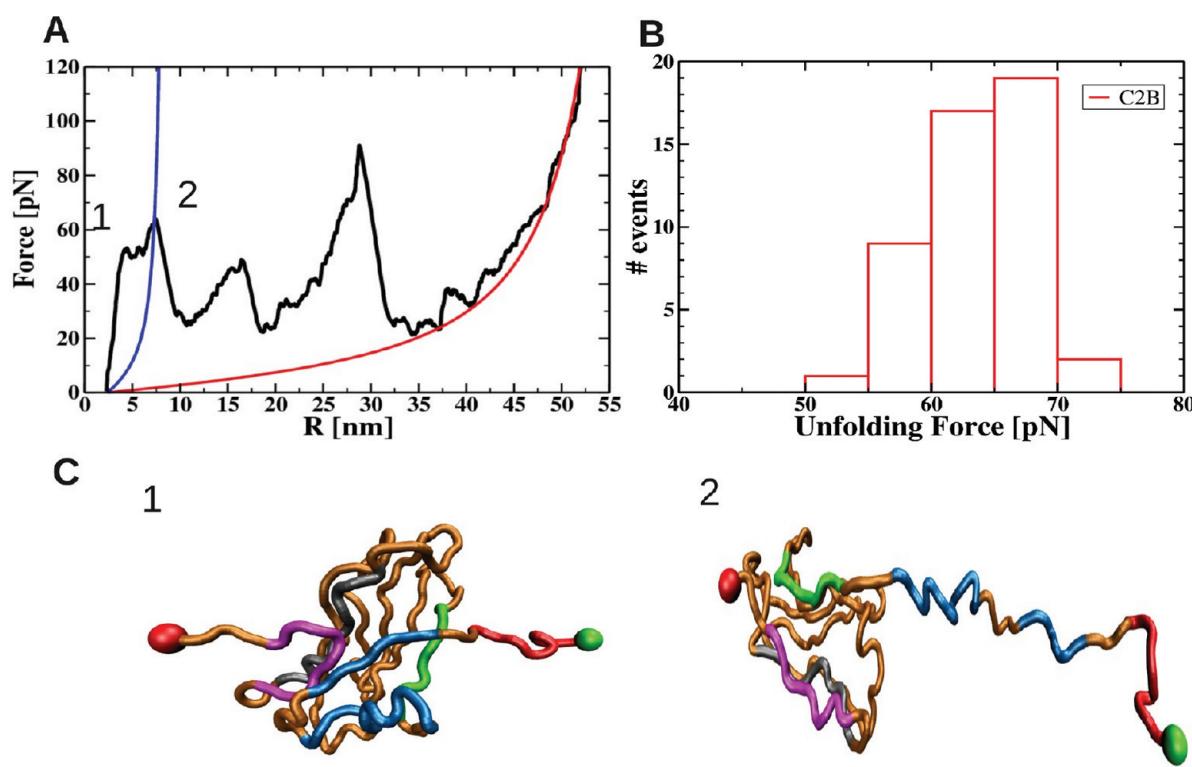
Figure 3. Force-induced unfolding of the isolated single C2B domain. Panels A and B show the theoretical FECs and the distribution of peak forces, respectively. Panel C: Structural snapshots 1 and 2, which correspond to the force peaks 1 and 2 observed in the FEC (panel A). Upon the first unfolding transition (peak 1), which corresponds to the disruption of binding contacts between the HA helix and the S8 strand and the rest of the C2B domain, we observe unraveling of the HB helix and partial detachment of the S1 strand (magenta), as shown in the conformation 1. This is followed by partial restructuring of the molecule, which leads to refolding of the S1 strand, and unfolding of the S8 strand and the HA helix at the C-term end of the chain (conformation 2).

simulations in Table 1). This prompted us to probe the mechanical stabilization of the C2B domain due to possible C2A−C2B domain interactions in the C2AB complex (C2AB simulations; Table 1).

The first peak in the force spectrum for the C2AB complex corresponds to a 95 pN force (Figure 4), and the unfolding reactions follow one of the three competing pathways. In the minor pathway 1 (4%), unfolding of C2AB starts with the disruption of favorable interactions stabilizing the C2A−C2B interface (Figure 4A). This is followed by a single-step unraveling of the C2A domain from its C-term end (Figure 4G, structure 1), resulting in an average unfolding force of 97.1 ± 6.4 pN (Figure 4D and Table 1). The transition reflected in peak 2 (Figure 4A), which corresponds to unfolding of the C2B domain at the C-term end, is also a single-step process (Figure 4G, structure 2). In pathway 2 (22%), the unfolding of the C2AB complex (Figure 4B) starts with the gradual unraveling of the C2A domain from the N-term end (Figure 4H, structure 1), while the C2A−C2B interface remains undisrupted. In pathway 2, the molecular transitions in the C2A domain are the same as those found in pathway 3 for the dimer C2A−C2A (section 4 in the Supporting Information), and the average peak force is 97.5 ± 6.7 pN (Figure 4E and Table 1). At this point, the exposure of hydrophobic residues in the intact part of C2A reaches 51.9%, rendering all the subsequent transitions experimentally undetectable. This implies that unfolding of C2A from the N-term end, when part of the C2AB complex, is a single-step process. Next, the C2B domain unfolds starting from the C-term

end (Figure 4H, structure 2). In the major pathway 3 (74%), the C2B domain unfolds prior to the C2A domain (Figure 4C). However, in pathway 3 as in pathway 1, the large first peak force of ∼95 pN (Figure 4F) corresponds to the disruption of the network of noncovalent binding contacts at the C2A−C2B junction. The mechanical tension accumulated in the C2A−C2B interface leads to a rapid loss of the hydrogen bonds between HB, S8, and HA in C2B, resulting in the unfolding of C2B (Figure 4I, structure 1). This is the last experimentally detectable force signal for unfolding of the C2B domain. The next detectable peak 2 (Figure 4C) corresponds to unfolding of the C2A domain from the C-term end, according to pathway 1 for the isolated C2A domain, which leads to formation of the intermediate state (Figure 4I, structure 2).

Without C2A−C2B Domain Interactions, C2A and C2B Contribute Equally to the Mechanical Stability of the C2AB Complex. Recent experiments[32] have shown that, due to flexibility of the C2A−C2B interface, the C2AB complex exists primarily in the "open" and "closed" states, in addition to partially associated transient conformations. To probe the role of C2A−C2B domain interactions in the mechanical response of the C2AB complex, we carried out pulling simulations for C2AB when the binding interactions between the C2A and C2B domains are switched off (C2A−C2B simulations; Table 1). We observed only two unfolding pathways. In 97% of the total of 92 trajectories, the C2B domain unfolded first (Figure 5B) at an average force of 59.7 ± 3.7 pN (Figure 5E; Table 1). This was followed by unfolding of the C2A domain (peaks 2 and 3 in
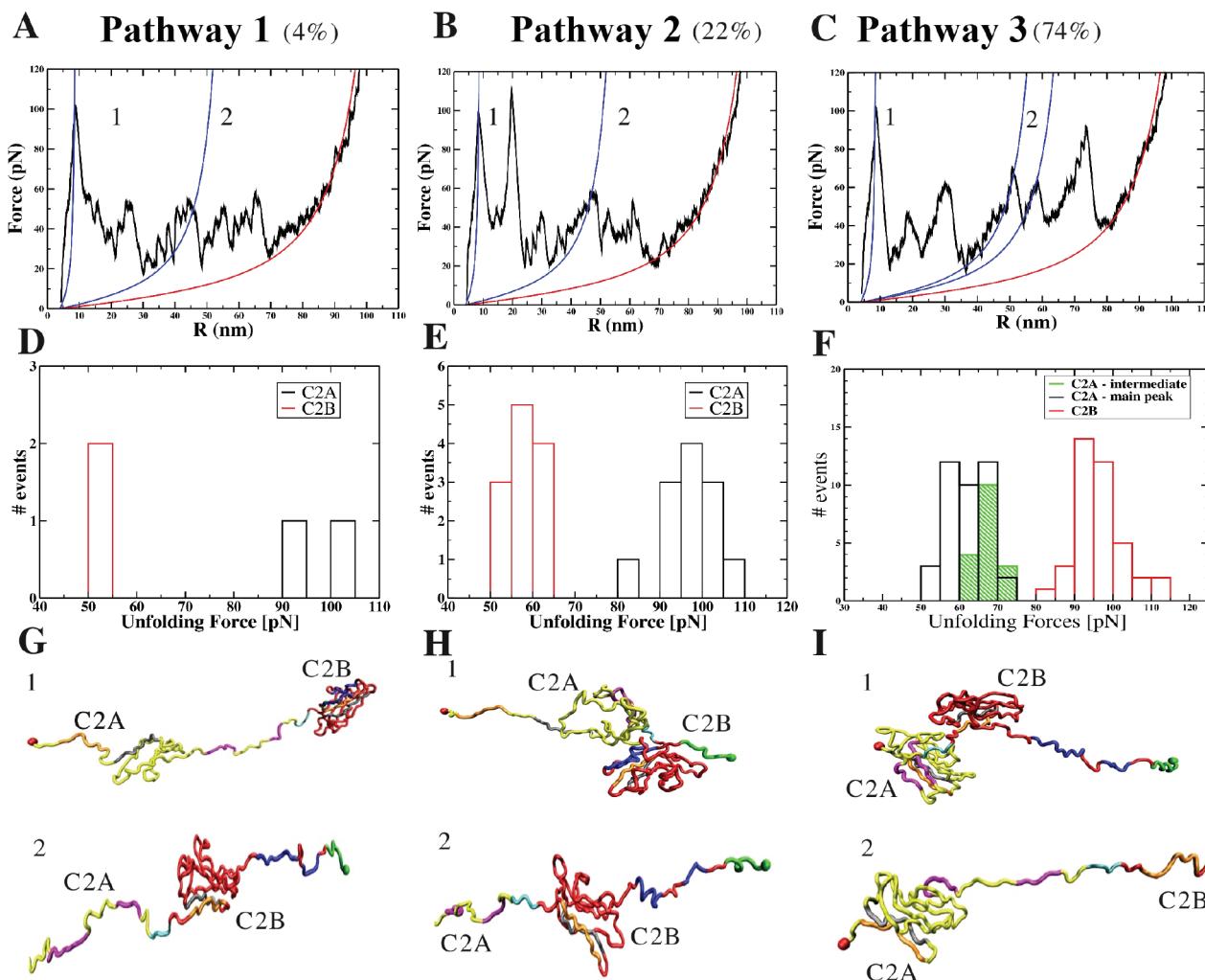
A Pathway 1 (4%) B Pathway 2 (22%) C Pathway 3 (74%)

Figure 4. The force-induced unfolding of the C2AB complex stabilized by the C2A−C2B association interface ("closed" state). Panels A−C display the theoretical force−extension profiles corresponding to the unfolding pathways 1−3, respectively. Panels D−F show the distribution of unfolding (peak) forces for each domain (C2A and C2B) and for each pathway 1−3, respectively. Panels G−I show the structural snapshots, which correspond to the force peaks 1 and 2 (panels A−C). For each pathway 1−3, structures 1 and 2 are labeled according to the force peaks they represent. In the majority of unfolding trajectories, unfolding of the closed conformation of the C2AB complex is initiated by the disruption of the noncovalent binding contacts stabilizing the C2A−C2B interface. This is followed by unraveling of the C2B domain (red) prior to unraveling of the C2A domain (yellow).

Figure 5B) at a similar average force of 61.9 ± 5.2 pN (Table 1). In the remaining 3% of trajectories, C2A unfolds first (Figure 5A). Interestingly, both domains unravel starting from their C-term ends as in pathway 1 for C2A (Figure 5C, structure 1) and for C2B (Figure 5C, structure 3), and in pathway 2 for C2B (Figure 5D, structure 1) and for C2A (Figure 5D, structure 2). In 37% of trajectories, we detected mixed character for opening of the C2A and C2B domains, which supports the notion that these domains have comparable mechanical resistance and implies that, in the absence of C2A−C2B domain interactions, C2A and C2B unfold independently. To provide more evidence for this notion, we performed implicit solvent models based simulations for the isolated single domains C2A and C2B (C2A(EEF1), C2B(EEF1), C2B(GBSW) simulations in Table 1; see, also, section 5 in the Supporting Information) and for the C2AB complex (C2AB-(EEF1) simulations in Table 1; see, also, section 6 in the Supporting Information). We found that, apart from the expected change in the magnitude of unfolding forces, the simulation data obtained using all-atomic modeling and coarse-grained

description (SOP) agree very well (sections 5 and 6 in the Supporting Information).

Effects of I27 Tandems on the Unfolding of Syt1. The results obtained from our pulling simulations for the C2AB complex are at odds with the experimental results of Oberhauser and co-workers[7] in a number of aspects. First, the C2B domain unravels first more often and, irrespective of the unfolding order, the first force signal is higher than the second. Second, in the absence of the C2A−C2B domain coupling, both domains C2A and C2B yield under similar force values. To understand the origin of this disagreement, we investigated the role of I27 domains in unfolding of the C2AB complex by carrying out pulling simulations on the tandem $(I27)_2-C2AB-(I27)_2$ of head-to-tail connected domains I27, C2A, and C2B. To construct the tandem and obtain the equilibrium tandem conformation, we used the protein-docking algorithm ZDOCK[38] (section 7 in the Supporting Information). We found that only the C2B domain forms binding contacts with the I27 domain, whereas the C2A domain is decoupled from I27 due to several steric hindrances.
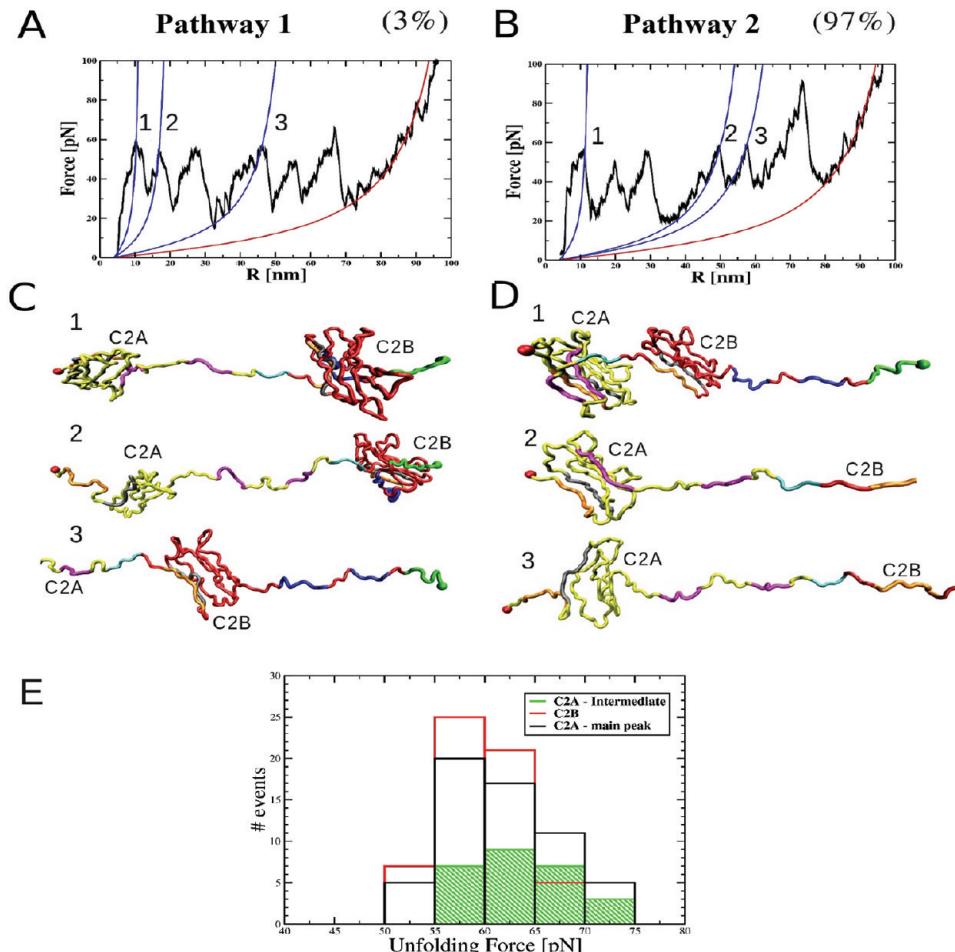
Figure 5. Force-induced unfolding of the C2AB complex with the C2A−C2B domain interactions switched off ("open" state). Panels A and B show the theoretical force−extension curves for the unfolding pathways 1 and 2, respectively. Corresponding to force peaks 1−3, structural snapshots 1−3, which show the conformational transitions in the domain C2A and C2B, are presented in panels C and D. In 97% of the trajectories, unfolding of the open conformation of the C2AB complex starts with the unraveling of the C2B domain at the C-term end (panels B and D, structure 1). This is followed by unraveling of the C2A domain at the C-term end (panels B and D, structures 2 and 3). Panel E: The histogram of unfolding (peak) forces showing that the critical forces for unfolding of the C2A and C2B domains are, indeed, comparable.

For tandem $(I27)_2$−C2AB−$(I27)_2$ in the presence of C2A−C2B domain interactions (C2AB−I27 simulations; Table 1), we observed three distinct unfolding pathways (Figure 6). These pathways are identical to the ones described previously for the C2AB complex. However, due to the C2B domain stabilization through coupling to the I27 domain, the probability of observing the C2B domain unfolding first decreases to 41% (Figure 6C). As in pathway 3 for the C2AB complex, C2B unfolds at the C-term end through unraveling of HB, S8, and HA (Figure 6I, structure 1). The two interfaces C2A−C2B and C2B−I27 open up at an average force of 96.7 ± 6.5 pN (Figure 6F). Next, C2A unfolds at an average force of 72.9 ± 7.0 pN (Figure 6C,F and Table 1) from the C-term end (Figure 6I, structure 2). In the remaining trajectories (59%), the C2A domain unfolds prior to the C2B domain. In pathway 1, now observed 45% of the time (Figure 6A), C2A unfolds at an average force of 92.7 ± 8.6 pN (Figure 6D and Table 1) at the C-term end, which is accompanied by the disruption of the C2A−C2B interface (Figure 6G, structure 1). Because the C2B−I27 interface remains intact, the critical force for the next unfolding transition (Figure 6A), i.e., unraveling of C2B at the C-term end (Figure 6G, structure 2),

increases to 116 ± 7.6 pN (Figure 6D and Table 1). Pathway 2, detected in 14% of trajectories (Figure 6B), corresponds to the single-step unfolding of C2A at the N-term end (Figure 6H, structure 1) at an average force of 98.8 ± 5.8 pN (Figure 6E and Table 1). Here, the first peak corresponds to the detachment of the C-term HB helix from the remaining part of C2B and to the disruption of the C2B−I27 interface. Interestingly, the HB helix refolds and binds back to C2B upon unfolding of C2A, and the C2B−I27 interface re-forms again (Figure 6H, structure 2). This refolding transition has two signatures in the force spectra (Figure 6B). First, the peak-to-peak distance between the first and second peaks is ∼40 nm, which is the full extension of C2A, and second, due to domain stabilization by the I27 domain, the critical force for unfolding of C2B increases to ∼120 pN (Figure 6E).

Our finding that the first unfolding transition, which occurs in C2A, becomes the dominant pathway (59%) points to the mechanical stabilization of the C-term end of the C2B domain by the I27 domain. This is also in accord with the recent experiments.[7] However, there is a significant difference between the experimental and simulation results regarding the larger
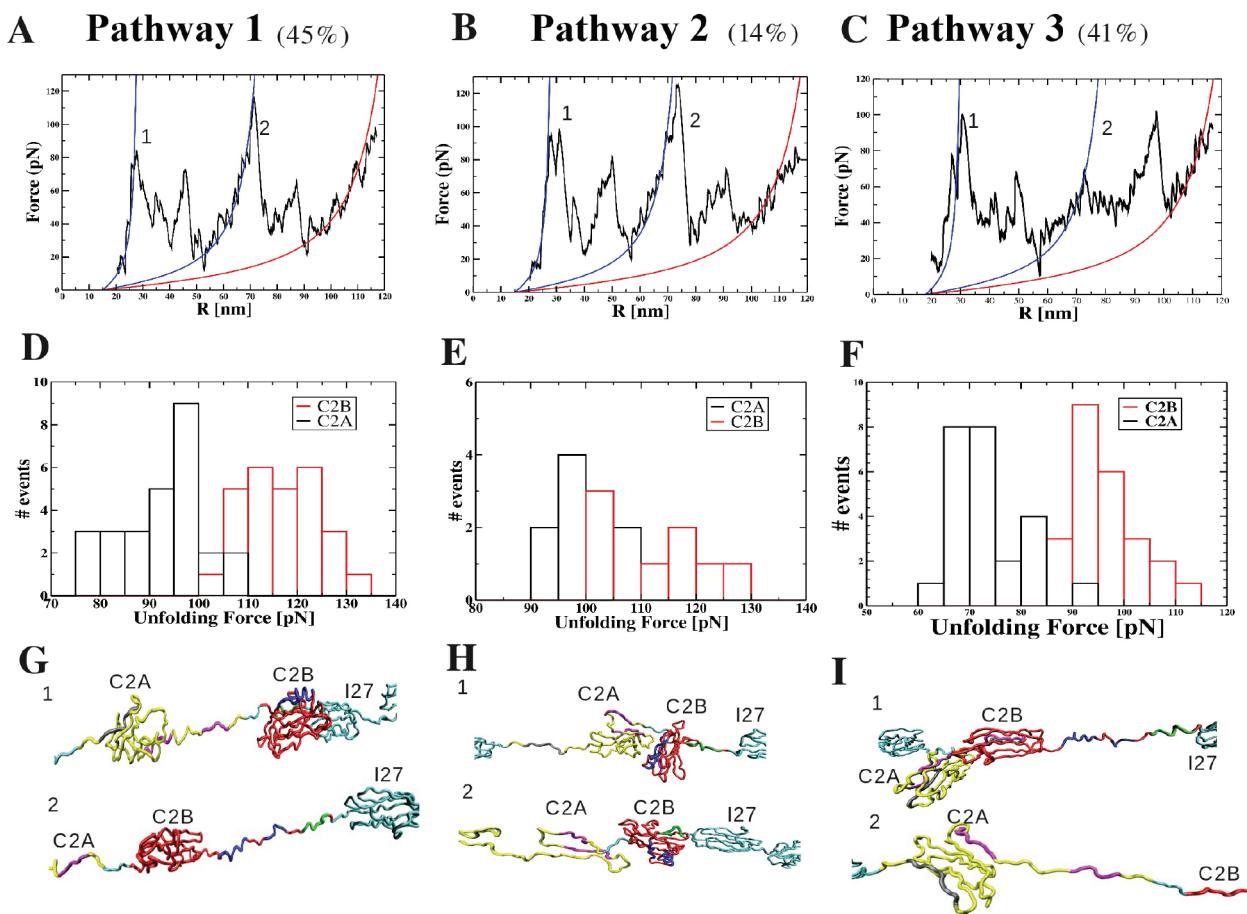
A Pathway 1 (45%)

B Pathway 2 (14%)

C Pathway 3 (41%)

Figure 6. Force-induced unfolding of the C2AB complex, stabilized by the C2A−C2B association interface ("closed" state), in tandem $(I27)_2$−C2AB−$(I27)_2$. Panels A−C show the theoretical FECs for pathways 1−3 detected. Although there is additional stabilization of the C2B−I27 interface, due to formation of binding contacts between the domains C2B and I27, these pathways are identical to pathways 1−3 for unfolding of the C2AB complex in the closed conformation (Figure 4). Panels D−F display the histograms of unfolding (peak) forces. Panels G−I show the structural snapshots for pathways 1−3. In pathway 1, now observed 45% of the time, the C2A−C2B interface opens first, while the C2B−I27 interface remains intact. This results in the first unfolding transition in the C2A domain at the C-term end (panels A and G). The probability of observing pathway 2 is reduced to 14%. Here, the C2A−C2B interface resists to pulling force, and C2A unravels first at the N-term end (panels B and H). In pathway 3 (41%), the C2A−C2B interface and the C2B−I27 interface open early on, and C2B is the first domain to unfold starting from the C-term end (panels C and I). In this pathway, the C2B domain yields to higher forces compared to the experimental force values reported in ref 7.

magnitude of unfolding forces for the C2A domain, observed in pulling simulations. The latter could be due to the disruption of the C2A−C2B interface when the C-term of C2A unfolds, or due to the change in the unfolding mechanism, i.e., from subsequent detachment of the secondary structure motifs in the direction from the C-term to the N-term end to progressive unraveling in the opposite direction. To discriminate between these potential scenarios, we ran pulling simulations for the tandem $(I27)_2$−C2AB−$(I27)_2$ with the C2A−C2B domain interactions switched off, while retaining interactions at the C2B−I27 interface (C2A−C2B−I27 simulations; Table 1). In all the simulation runs (Figure 7), the unfolding process starts at the C-term end of the C2A domain at an average force of 69.0 ± 7.2 pN (peak 1 in Figure 7A and structure 1 in Figure7C). The C2B domain unravels only after the C2A domain has unfolded (Figure 7C, structure 3). Due to the C2B−I27 domain interactions, the average unfolding force for C2B is now 117.2 ± 8.5 pN (peak 3 in Figure 7A, peak 2 in Figure 7B, and Table 1), in agreement with experiments.[7] Moreover, due to unraveling of the S8 strand, 33.7% of the time (pathway 1) C2A unfolds through the

formation of an intermediate state (peak 1 in Figure 7A and structure 1 in Figure 7C), i.e., following pathway 1 observed in pulling simulations for the isolated single C2A domain (C2A simulations in Table 1; see, also, Figure 2A). In the remaining 66.3% of trajectories (pathway 2), C2A unfolds following pathway 2 detected in the C2A simulations (peak 1 in Figure 7B). Again, this is consistent with the experimental results for unfolding of the C2A domain when part of the C2AB complex. Interestingly, the force signal for formation of the intermediate state is controlled by the S8 strand in C2A. Indeed, for the tandem $(I27)_2$−C2AB−$(I27)_2$ with "open" C2AB configuration, when the energy of noncovalent interactions between the S8 strand and the rest of the C2A domain is reduced by 30% (from 0.9 to 0.6 kcal/mol), on the basis of the spread of force values resulting from our EEF1 simulations for the C2A domain (panel E in Figure SI4 in the Supporting Information), we recover the experimental results[7] for the magnitude of unfolding force for the intermediate state observed for C2A (first peak in panel A in Figure SI10, Supporting Information; see, also, Table 1).
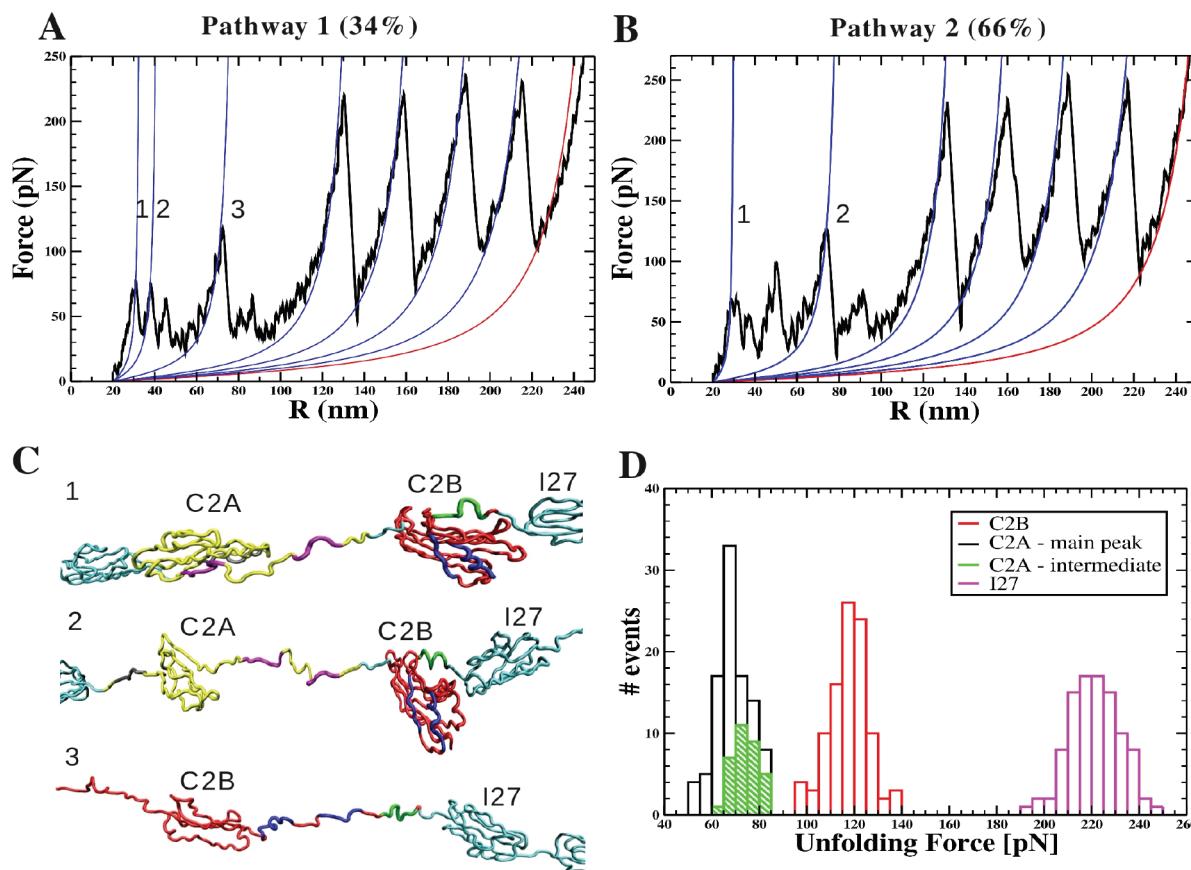
10142

dx.doi.org/10.1021/jp2025945 |*J. Phys. Chem. B* 2011, 115, 10133−10146

Figure 7. Force-induced unfolding of the open conformation of the C2AB complex in tandem $(I27)_2-C2AB-(I27)_2$. Panels A and B show the theoretical FECs for pathways 1 and 2. When the C2A−C2B interface is open and the C2B domain (red) is stabilized by the I27 domain, the C2A domain (yellow) always unfolds first (100% of the time) at the C-term end (panels A and B). Panel C: Structural snapshots 1−3, which represent the conformational transitions in the domains C2A and C2B and correspond to force peaks 1−3 in panel A. Panel B shows pathway 2 for unfolding of C2A (peak 1; same pathway 2 shown in Figure 2), and C2B (peak 2; unfolding at the C-term end). Panel D: Histogram of peak forces showing that the force required to unravel the C2A domain is significantly lower than the unfolding force for the C2B domain, in agreement with the AFM experiments.[7]

■ DISCUSSION AND CONCLUSIONS

Despite its crucial importance for neuronal function, many functional aspects of Syt1 are not yet understood, and the molecular mechanism, by which Syt1 triggers SNARE-mediated fusion, is not fully resolved.[39] A great challenge in elucidating this mechanism is the lack of understanding of the connection between the structure of the C2AB complex (C-terminal cytoplasmic region of Syt1), subject to the external mechanical activation, and its function. To date, two scenarios have been proposed by researchers regarding the degree of cooperation between the domains C2A and C2B in Syt1. According to the first scenario, the C2A and C2B domains act independently, performing their functions as separate modules. The second scenario is based on the notion that the C2A and C2B domains must cooperate for Syt1 to perform its function. On the one hand, there is a large body of experimental evidence that supports the first scenario, including recent NMR experiments with site-directed spin labeling.[39,40] These studies have shown no detectable interactions between the C2A and C2B domains, which are also known to have different biochemical properties. For example, many synaptic components such as Ca^{2+} channels and other copies of Syt1 bind to C2B, but not to C2A.[41]

On the other hand, the crystal structure of the C2AB complex of human Syt1 revealed the existence of the C2A−C2B association interface between the C2A and C2B domains.[6] This finding provides structural evidence for the second scenario further supported by recent experiments, in which the C2A and C2B domains were found to participate in the Ca^{2+}-triggered simultaneous membrane penetration.[41] Upon binding Ca^{2+} ions, both C2 domains partially penetrate into the membrane that contains anionic phospholipids. Using site-directed fluorescent probes to monitor the penetration of the C2 domains into phosphatidylserine rich lipid bilayers, Chapman and collaborators[41] have found that membrane penetration by the cytoplasmic region of Syt1 shows significant resistance to changes in ionic strength. Chapman and collaborators[41] also found that the ability of an isolated single C2B domain to bind to membranes can be severely disrupted by a small change in ionic strength, and that in the presence of the C2A domain the penetration depth for both domains increases. Doubling the length of the linker connecting the C2A and C2B domains leads to reduced interactions of the C2AB portion of Syt1 with the SNARE complex. Hence, there is an ample body of experimental evidence that points to close cooperation and, possibly, direct coupling between the C2A and C2B domains in the C2AB complex.[42]

Employing AFM-based dynamic force spectroscopy, Oberhauser and collaborators[7] have predicted a complex unfolding pattern for the C2A domain, including formation of an

intermediate partially unfolded state. This pattern has been observed in AFM experiments on other proteins with a similar native fold, including the FnII10 domain.[5] Oberhauser and collaborators have also concluded that the C2B domain is the most mechanically stable domain in Syt1, resisting pulling forces twice as large as the forces for the C2A domain. Although these studies have provided valuable information about the physical properties of the C2AB complex, it remains unclear as to what makes the C2AB complex highly resistant mechanically, and why the C2B domain is more mechanically stable compared to its C2A partner. The latter finding is somewhat striking in view of the large structural similarity shared by the C2A and C2B domains. Conceivably, C2B might be stabilized by C2A through domain interactions at the C2A−C2B junction, but this domain stabilization effect has not yet been characterized.

In this paper, we carried out pulling simulations for Syt1-derived systems of different complexity from isolated single C2 domains C2A and C2B, to the C2A dimer C2A−C2A, to the C2AB complex, and to the tandem $(I27)_2$−C2AB−$(I27)_2$. We obtained structural information, at the residue level, about the microscopic transitions underlying the force-induced elongation and unfolding of the domains C2A and C2B and characterized the unfolding pathways for the C2AB complex. We employed combined all-atom MD simulations in implicit water (EEF1 and GBSW models) and Langevin simulations on graphics processors using a coarse-grained description of the Syt1 polypeptide chain (SOP model). The EEF1 model based simulations have been used to obtain the parametrization necessary for the SOP model and, together with the GBSW model based simulations, to validate the results of Langevin simulations. Importantly, the SOP-model based description in conjunction with Langevin simulations on a GPU have enabled us to perform dynamic force measurements in silico in the experimental centisecond time scale by applying realistic force-loads (pulling speeds of 2.5 μm/s) used in AFM assays in vitro. These efforts allowed us to compare directly the results of pulling simulations with the experimental force data and to reach to experimentally testable conclusions.

We found that the isolated C2A domain unfolds following one of two competing pathways, in very good agreement with the results of Fuson et al.[7] On the basis of the structural details resolved in our simulations, we propose that, in both pathways, unraveling of the C2A domain is initiated by the detachment of the S8 strand from the C-term end. In the major pathway, C2A unfolded gradually from the C-term end, whereas in the minor pathway we observed unraveling of the N-term strand S1 and the C-term strand S7. This leads to formation of the intermediate state at a molecular extension of ∼7 nm, which might be the intermediate conformation detected in experiments.[7] For the C2A dimer (C2A−C2A), we found an additional (third) pathway, according to which the S1 strand at the N-term unfolds first through unzipping from the S8 strand at a force of ∼60 pN, which also agrees with experiments.[5] Our theoretical findings can be tested experimentally using C2A constructs that contain disulfide bonds between positions in the strands S1 and S2 (strands S8 and S7) to constrain the N-term (C-term) end of C2A.[20] Simulations carried out for the isolated C2B domain suggest that this domain unravels following a single pathway, with no intermediate species. Unfolding of the C2B domain, initiated at the C-term end, involves unraveling of two α-helices, HA and HB, and one β-strand, S8. On the basis of these results, we hypothesize that mechanical stability of C2B is determined by

Table 2. Numerical Estimates of the Thermodynamic Parameters for the Forced Unfolding of the C2 Domains at T = 300 K

domain	w, kcal/mol	ΔH, kcal/mol	$T\Delta S$, kcal/mol
C2A (I)[a]	53.7 ± 5.9	36.6 ± 10.4	−17.1 ± 5.9
C2A	342.1 ± 36.9	239.9 ± 9.3	−102.2 ± 36.9
C2B	390.7 ± 23.2	315.4 ± 11.1	−75.3 ± 23.2

[a] Thermodynamic quantities characterizing formation of the intermediate state in C2A (Figure 2A).

the physical properties of its C-term secondary structure motifs, which resist to pulling forces up to ∼60 pN.

To provide thermodynamic measures of unfolding for the C2 domains, we estimated the total energy change and work performed on each system. In each case, we compared the energy for the final (fully extended) state with the energy for the native (folded) state. Neglecting energy dissipation, we evaluated the total work (w) by performing the numerical integration of the area under the force−distance curves (Figure 2A and B, and Figure 3A). In our *NPT* pulling simulations, in which we maintained the conditions of constant number of particles (N), pressure (P), and temperature (T), the total work performed on the system is expended to change the Gibbs free energy $\Delta G = \Delta H − T\Delta S$. Numerical values of the enthalpy change ΔH due to the disruption of the native contacts stabilizing the native state, work (w), and entropy change $T\Delta S$ (chain elongation) are accumulated in Table 2. Because all the pulling simulations have been carried out under nonequilibrium conditions, these characteristics should be viewed as rough estimates of the equilibrium thermodynamic quantities. The similarity of the w and ΔH values obtained for the C2A and C2B domains support the notion that these domains are comparable in terms of their mechanical stability. This finding correlates well with results from recent thermal denaturation studies, which showed that both C2A and C2B domains melt at the same temperature, $T = \sim$60 °C.[43] All-atomic MD simulations, carried out at a much faster pulling speed, confirmed the main results from SOP-model based simulations. They also showed that formation of non-native contacts does not change the kinetic pathways for unfolding of neither C2A nor C2B and has little or no effect on the distribution of unfolding forces. This is because these transient contacts are too short-lived to be relevant in the experimental 10−40 ms time scale. In summary, on the basis of the results obtained, we conclude that the isolated C2 domains in Syt1 have similar mechanical properties. We anticipate that this result will motivate future single-molecule studies of the isolated C2B domain to resolve the molecular origin and extent of the mechanical stability of this domain. This is highly important, because C2B is capable of performing its function independently from the rest of the Syt1 molecule.[8]

Our results from EEF1- and SOP-model based simulations for the C2AB complex (not connected to the $(I27)_2$ constructs) are at odds with the conclusion of Fuson et al. that C2A is the weakest domain mechanically.[7] We showed that the experimental results of Fuson et al. are reproduced almost quantitatively when the $(I27)_2$ constructs flanking the C2AB complex in tandem $(I27)_2$−C2AB−$(I27)_2$ are described explicitly. Moreover, we found that, in tandem $(I27)_2$−C2AB−$(I27)_2$, the I27 domain provides additional stabilization for the C2B domain through domain interactions at the C2B−I27 interface, even

when the C2A–C2B domain interactions are turned off. The mechanical stabilization of the C2B domain by way of interactions with other proteins has also been observed in a recent single-molecule FRET (smFRET) experiment.[32] In that study, the SNARE complex has been found to bind to the same portion of C2B that accommodates docking of the I27 domain in our simulations.[32] Syt1 is known to bind simultaneously to the membrane and to the SNARE complexes anchored at the membrane leading to formation of a quaternary complex. These interactions help create negative curvature on the membrane, which results in the membrane bending and fusion.[44] In this picture, protein–protein interactions between the C2B domain and the SNARE complex confers rigidity to the C2AB complex, allowing it to sustain large mechanical tension exerted by the curved membrane.[4]

The FRET data also revealed that the SNARE-bound Syt1 complex has a flat configuration, in which there are no contacts between the C2A and C2B domains.[32] Moreover, Choi et al. detected the presence of at least two competing configurations for the isolated C2AB complex, which they assigned to the closed and open states. As there are occasional rapid transitions between these states, Choi et al. concluded that the C2 domains in Syt1 perform relative random motions when not bound to the SNARE complex.[32] The flat configuration resembles the open conformation of the C2B–I27 fragment used in pulling simulations for tandem $(I27)_2$–C2AB–$(I27)_2$. Our own results for this construct show that, when C2B is mechanically coupled to I27, the most probable unfolding force for the C2A domain is ∼60 pN, while for the C2B domain it is ∼120 pN. These force values land in the range of forces measured by Fuson et al.[7] The resulting molecular elongation of ∼40 nm (for C2A) and ∼45 nm (for C2B) also agrees well with the experimental estimates of Fuson et al.[7] Our results also indicate that, upon docking of I27 to C2B when Syt1 (C2AB complex) is in the open conformation (flat configuration in smFRET studies of Choi et al.), the entire "bottom" surface of C2B becomes available for association with the I27 domain. Here, the number of binary interactions between the C2B and I27 domains increases from 20 contacts for the C2AB complex in the closed conformation to 36 contacts. Hence, taken together, our results and the recent smFRET data indicate strongly that the most likely state of the C2AB complex studied in the AFM experiments of Fuson et al.[7] is the open conformation. Structural analysis revealed that strong C2A–C2B domain interactions in the C2AB complex induce unraveling of the C2A domain from the N-term end. This transition occurs under higher unfolding forces compared to forces for opening of C2A from the C-term end, which is the unfolding route for the isolated C2A domain. Hence, in the presence of cooperative domain interactions with the C2B domain, the C2A domain unravels following an entirely different pathway. Thus, the detachment of the S1 strand, which occurs first, is due to presence of another C2A domain as in the C2A dimer, or due to formation of stable C2A–C2B association interface (C2AB complex). In contrast, in the isolated C2A domain, the S8 strand yields first to an applied pulling force.

In conclusion, our results provide structural evidence for the mechanical coupling and cooperative behavior of the C2A and C2B domains in Syt1 subject to external physical factors. When separated from each other, both C2 domains are likely to show only modest mechanical resistance. Hence, we propose that, to sustain large mechanical tension due to buckling of the plasma membrane (∼120 pN,[4]), the C2A and C2B domains must associate or must gain additional stabilization by binding to a third party. The latter scenario can be realized, e.g., through protein–protein interactions between the Syt1 protein and the SNARE complex.[32] This scenario is further supported by the notion that the HA helix, which mediates domain interactions between Syt1 and SNARE, enhances the mechanical stability of C2B.[7] Our own results indicate that the order of unfolding events in the C2A domain is mostly determined by the mechanical properties of the S8 strand.

Additional insights into the role of the S8 strand could be obtained by combining the bioinformatics approach and structural similarity analysis as exemplified by Jimenez et al.[45] Their study revealed that the S8 strand is divergent in the family of C2 domains in general and, particularly, in the C2A domain, in which Trp259 is the only conserved position. In a sense, the lack of conservation might be due to lower functional importance of this fragment. Our own results provide more evidence in support of this notion, because the S8 strand in the isolated C2A domain unravels at relatively weak forces (∼35–40 pN). On the other hand, the S1 strand, which is more conserved in the C2A domains (30% of residues in S1) but divergent in the family of C2 domains,[45] unravels at higher forces (∼90 pN). Hence, there seems to be a direct correlation between the degree of evolutionary conservation and mechanical stability for the secondary structure elements in the C2A domain.

■ ASSOCIATED CONTENT

ⓢ **Supporting Information.** Additional details of the energy function and information about the simulation setup for the SOP model and implicit solvent models. Results for unfolding of the C2A dimer obtained using the SOP model, and analysis of the implicit solvent simulations and docking are included along with supporting figures. A table summarizing the details of simulation protocols is included. This material is available free of charge via the Internet at http://pubs.acs.org/.

■ AUTHOR INFORMATION

Corresponding Author
*E-mail: Ruxandra.Dima@uc.edu. Phone: +1 513 5563961. Fax: +1 513 5569239.

■ ACKNOWLEDGMENT

■ REFERENCES

(1) Chernomordik, L. V.; Kozlov, M. M. *Nat. Struct. Mol. Biol.* **2008**, *15*, 675–683.

(2) Martens, S.; Kozlov, M. M.; McMahon, H. T. *Science* **2007**, *316*, 1205–1208.

(3) Herrick, D. Z.; Sterbling, S.; Rasch, K. A.; Hinderliter, A.; Cafiso, D. S. *Biochemistry* **2006**, *45*, 9668–9674.

(4) Takahashi, H.; Shahin, V.; Henderson, R. M.; Takeyasu, K.; Edwardson, J. M. *Biophys. J.* **2010**, *99*, 2550–2558.

(5) Carrion-Vazquez, M.; Oberhauser, A. F.; Fisher, T. E.; Marszalek, P. E.; Li, H.; Fernandez, J. M. *Prog. Biophys. Mol. Biol.* **2000**, *74*, 63–91.

(6) Fuson, K. L.; Montes, M.; Robert, J. J.; Sutton, R. B. *Biochemistry* **2007**, *46*, 13041–13048.

(7) Fuson, K. L.; Ma, L.; Sutton, R. B.; Oberhauser, A. F. *Biophys. J.* **2009**, *96*, 1083–1090.

(8) Gaffney, J. D.; Dunning, F. M.; Wang, Z.; Hui, E.; Chapman, E. R. *J. Biol. Chem.* **2008**, *283*, 31763–31775.

(9) Lu, H.; Isralewitz, B.; Krammer, A.; Vogel, V.; Schulten, K. *Biophys. J.* **1998**, *75*, 662–671.

(10) Lu, H.; Schulten, K. *Proteins* **1999**, *35*, 453–463.

(11) Zhmurov, A.; Dima, R. I.; Kholodov, Y.; Barsegov, V. *Proteins* **2010**, *78*, 2984–2999.

(12) Lazaridis, T.; Karplus, M. *Proteins* **1999**, *35*, 133–152.

(13) Hyeon, C.; Dima, R. I.; Thirumalai, D. *Structure* **2006**, *14*, 1633–1645.

(14) Paci, E.; Karplus, M. *Proc. Natl. Acad. Sci. U. S. A.* **2000**, *97*, 6521–6526.

(15) Paci, E.; Vendruscolo, M.; Karplus, M. *Biophys. J.* **2002**, *83*, 3032–3038.

(16) Qin, Z.; Kreplak, L.; Buehler, M. J. *PLoS One* **2009**, *4*, e7294–13.

(17) Im, W.; Lee, M.; C., B., III. *J. Comput. Chem.* **2003**, *24*, 1691–1702.

(18) Dima, R. I.; Joshi, H. *Proc. Natl. Acad. Sci. U. S. A.* **2008**, *105*, 15743–15748.

(19) Hyeon, C.; Onuchic, J. N. *Proc. Natl. Acad. Sci. U. S. A.* **2007**, *104*, 2175–2180.

(20) Mickler, M.; Dima, R. I.; Dietz, H.; Hyeon, C.; Thirumalai, D.; Rief, M. *Proc. Natl. Acad. Sci. U. S. A.* **2007**, *104*, 20268–20273.

(21) Tehver, R.; Thirumalai, D. *Structure* **2010**, *18*, 471–481.

(22) Hyeon, C.; Jennings, P. A.; Adams, J. A.; Onuchic, J. N. *Proc. Natl. Acad. Sci. U. S. A.* **2009**, *106*, 3023–3028.

(23) Lin, J. C.; Thirumalai, D. *J. Am. Chem. Soc.* **2008**, *130*, 14080–14084.

(24) Chen, J.; Dima, R. I.; Thirumalai, D. *J. Mol. Biol.* **2007**, *374*, 250–266.

(25) Hyeon, C.; Lorimer, G. H.; Thirumalai, D. *Proc. Natl. Acad. Sci. U. S. A.* **2006**, *103*, 18939–18944.

(26) Li, M. S. *Biophys. J.* **2007**, *93*, 2644–2654.

(27) Sulkowska, J. I.; Cieplak, M. *Biophys. J.* **2008**, *95*, 3174–3191.

(28) Seiler, L.; Carmean, D.; Spran, E. *J. Comput. Chem.* **2007**, *28*, 2618–2640.

(29) Phillips, J. C.; Stone, J. E.; Schulten, K. Adapting a message-driven parallel application to GPU-accelerated clusters. *SC '08: Proceedings of the 2008 ACM/IEEE conference on Supercomputing*; IEEE Press: Piscataway, NJ, 2008; pp 1–9.

(30) Friedrichs, M. S.; Eastman, P.; Vaidyanathan, V.; Houston, M.; Legrand, S.; Beberg, A. L.; Ensign, D. L.; Bruins, C. M.; Pande, V. S. *J. Comput. Chem.* **2009**, *30*, 864–872.

(31) Dietz, H.; Berkmeier, F.; Bertz, M.; Rief, M. *Proc. Natl. Acad. Sci. U. S. A.* **2006**, *103*, 12724–12728.

(32) Choi, U. B.; Strop, P.; Vrljic, M.; Chu, S.; Brunger, A. T.; Weninger, K. R. *Nat. Struct. Mol. Biol.* **2010**, *17*, 318–325.

(33) Joshi, H.; Momin, F.; Haines, K. E.; Dima, R. I. *Biophys. J.* **2010**, *98*, 657–666.

(34) Veitshans, T.; Klimov, D. K.; Thirumalai, D. *Folding Des.* **1996**, *2*, 1–22.

(35) Holm, L.; Sander, C. *J. Mol. Biol.* **1991**, *218*, 183–194.

(36) Kolinski, A.; Godzik, A.; Skolnick, J. *J. Chem. Phys.* **1993**, *98*, 7420–7433.

(37) Li, H.; Oberhauser, A.; Fowler, S.; Clarke, J.; Fernandez, J. *Proc. Natl. Acad. Sci. U. S. A.* **2000**, *97*, 6527–6531.

(38) Chen, R.; Li, L.; Weng, Z. *Proteins* **2003**, *52*, 80–87.

(39) Huang, H.; Cafiso, D. S. *Biochemistry* **2008**, *47*, 12380–12388.

(40) Arac, D.; Chen, X.; Khant, H. A.; Ubach, J.; Ludtke, S. J.; Kikkawa, M.; Johnson, A. E.; Chiu, W.; Sudhof, T. C.; Rizo, J. *Nat. Struct. Mol. Biol.* **2006**, *13*, 209–217.

(41) Hui, E.; Bai, J.; Chapman, E. R. *Biophys. J.* **2006**, *91*, 1767–1777.

(42) Bai, J.; Wang, C.-T.; Richards, D. A.; Jackson, M. B.; Chapman, E. R. *Neuron* **2004**, *41*, 929–942.

(43) Shin, O.-H.; Xu, J.; Rizo, J.; Sudhof, T. C. *Proc. Natl. Acad. Sci. U. S. A.* **2009**, *106*, 16469–16474.

(44) Rizo, J.; Rosenmund, C. *Nat. Struct. Mol. Biol.* **2008**, *15*, 665–674.

(45) Jimenez, J. L.; Smith, G. R.; Contreras-Moreira, B.; Sgouros, J. G.; Meunier, F. A.; Bates, P. A.; Schiavo, G. *J. Mol. Biol.* **2003**, *333*, 621–639.

(46) Humphrey, W.; Dalke, A.; Schulten, K. *J. Mol. Graph.* **1996**, *14*, 33–38.